The Gold Dihydride Molecule, AuH_2: Calculations of Structure, Stability, and Frequencies, and the Infrared Spectrum in Solid Hydrogen†

Lester Andrews* and Xuefeng Wang

Department of Chemistry, University of Virginia, P.O. Box 400319, Charlottesville, Virginia 22904-4319

Laurent Manceron

LADIR/Spectrochimie Moléculaire CNRS UMR 7075- Université Pierre et Marie Curie, case 49, 4 place Jussieu, 75252 Paris, France

K. Balasubramanian

Department of Applied Science, University of California, Davis, Livermore, California 94550; Chemistry and Materials Science Directorate, Lawrence Livermore National Laboratory, University of California, Livermore, California 94550; Glenn T. Seaborg Center, Lawrence Berkeley Laboratory, University of California, Berkeley, California 94720

Received: September 25, 2003; In Final Form: October 29, 2003

The novel AuH_2 molecule has been formed in solid hydrogen by reactions of excited gold atoms from laser ablation and irradiation after thermal evaporation. The X^2B_2 ground state of the AuH_2 molecule is separated by a 53 kcal/mol barrier from the $Au(^2D) + H_2$ decomposition products and it is 27 kcal/mol more stable than $Au(^2D) + H_2$. The bending modes of AuH_2, AuHD, and AuD_2 have been observed at 638.1, 570.6, and 457.0 cm^{-1}. These frequencies and the lack of infrared intensity in the stretching modes are in agreement with the results of relativistic ECP DFT, MP2, and CCD calculations. The computed bending potential energy surfaces of three electronic states of AuH_2 using CASSCF/MRSDCI methods reveal that there is a barrier for decomposition of the X^2B_2 ground state to $Au(^2S) + H_2$.

Introduction

Although gold is noble, excited gold is reactive; however, gold is the least reactive of the coinage metals.[1] Despite this, AuH is the most stable of Group 11 monohydrides because of relativistic effects.[2,3] The next gold hydride AuH_2 is computed to be a physically stable molecule and to have two unusual properties: AuH_2 is higher in energy than $Au + H_2$ and the Au−H stretching modes have low but the H−Au−H bending mode high infrared intensities.[4−6] Gold trihydride was first predicted to be T-shaped,[7] but two groups have calculated AuH_3 to be a transition state and stable as $(H_2)AuH$, which is the dihydrogen complex of AuH.[8,9] In this laboratory, we have observed the $(H_2)AuH$ complex in solid argon, neon, and hydrogen and found AuH_3 to be trapped as the $(H_2)AuH_3$ complex.[5,10]

Gold(II) is an unusual oxidation state. Such compounds are rare, and many formally divalent gold complexes are in fact mixed valence Au(I)/Au(III) compounds. Most Au(II) compounds contain Au−Au bonds.[1] However, the AuO molecule has been observed in two matrix isolation studies[11,12] and the $AuCl_2$ molecule has been characterized by photodetachment of $AuCl_2^-$ in a recent mass and photoelectron spectroscopic and theoretical investigation.[13] The $AuCl_2$ molecule and $AuCl_2^-$ anion are both stable to dissociation and the 4.60 ± 0.07 eV electron affinity measured for $AuCl_2$ attests the stability of $AuCl_2^-$.

We report here another example of the close working relationship between quantum chemistry and matrix isolation spectroscopy, namely, AuH_2, a molecule formed in the excited $Au(^2P)$ and H_2 reaction, stabilized by relativistic effects, and separated by an energy barrier from its lower energy $Au + H_2$ decomposition products.

Schaefer was among the first theorists to address important experimental molecular subjects such as methylene using modern quantum chemistry.[14,15] In particular, the Schaefer group established an effective working relationship with matrix isolation spectroscopy both in supporting earlier reports[16,17] and in describing new molecular species for future experimental investigation.[18,19]

Experimental and Theoretical Methods

Two experimental approaches were used to generate gold atoms for reaction with pure hydrogen, namely, laser ablation and thermal evaporation. The former employs 1064 nm from a YAG laser (10−20 mJ per 10-ns pulse at 10 Hz) focused onto a rotating gold target and the latter uses a shielded tungsten filament to evaporate gold at approximately 1900 °C.[20−24] Both methods condense gold atoms with 2−3 millimoles of pure normal H_2 on substrates cooled to near 3.5 K by closed-cycle refrigerators. Infrared spectra are recorded, samples are subjected to filtered mercury arc radiation, annealing cycles, and more spectra are recorded.

Complementary density functional theory (DFT) calculations were performed using the Gaussian 98 program,[25] the BPW91 and B3LYP density functionals,[26,27] the 6-311++G(d,p) and

† Part of the special issue "Fritz Schaefer Festschrift".

* Address correspondence to this author. E-mail: lsa@virginia.edu.

10.1021/jp036864z CCC: $27.50
Published on Web 02/11/2004

6-311++G(3df, 3dp) basis sets[28] for H and SDD and LANL2DZ effective core potentials and basis sets for gold as given in Gaussian 98.[3,29] Vibrational frequencies were computed analytically from the potential energy surface in the harmonic approximation at the optimized structures: the calculated frequencies reported here are not scaled. The BPW91 functional and LANL2DZ pseudopotential have been recommended for Group 11 metal-containing molecules after comparison of results using several methods although the B3LYP functional works almost as well.[30] The LANL2DZ basis is only of double-ζ quality and without 4f functions, and thus it is less accurate than the treatment described in the ensuing paragraph.

We have also computed both the potential energy surfaces and the vibrational frequencies using higher level methods. Recognizing that both relativistic effects[31,32] and multireference techniques are important particularly for the study of the potential energy surfaces, we have employed a complete active space multiconfiguration self-consistent field method as a starting point. We used the relativistic effective core potential methods[31] to represent the gold atom with $5d^{10}6s^1$ shells as the valence space replacing the remaining 68 electrons by RECPs of Ermler and co-workers. Since the first excited state of the gold atom arises from the $5d^9 6s^2$ configuration and the second excited state arises from the $5d^{10}6p^1$ configuration, it is important to include all 5d, 6s, and 6p orbitals in the active space of the CASSCF. Thus, our active space included five a_1 orbitals, three b_2 orbitals, two b_1 orbitals, and one a_2 orbital and all 13 valence electrons of AuH_2. These 13 electrons were distributed in all possible ways among the active orbitals. We employed an extended (3s3p4d1f) basis set for the gold atom and a triple-ζ + polarization basis set for the hydrogens.

We carried out multireference singles + doubles configuration interaction (MRSDCI) computations following the CASSCF. The MRSDCI computations again correlated all 13 electrons and included all configurations in the CASSCF with absolute coefficients more than or equal to 0.01. Thus, the MRSDCI typically included single + double excitations from 65 reference configurations which resulted in up to 3.4 million configurations. The MRSDCI thus included dynamical electron correlation effects. Since MRSDCI method is not size consistent, dissociation energies were computed carefully using a supermolecular computation in which the Au−H distances were set to 10 Å.

The vibrational frequencies were computed using the coupled cluster (CCD) method as well as the MP2 method in the same gold basis set and H aug-cc-pvtz basis sets. These frequencies together with the IR intensities were compared with both experiment and DFT levels of theory. All the CASSCF/MRSDCI computations were made using Balasubramanian's[31,32] modified version of ALCHEMY II codes,[33−35] while the MP2 and CCD computations were made using the Gaussian package.[25]

Results and Discussion

Gold and pure hydrogen reaction products will be reported using two methods of generating gold atoms. Gold dihydride calculations will be presented at the DFT/ECP and relativistic MP2, CCD, and CASSCF/MRSDCI levels of theory to support the identification of the novel AuH_2 molecule.

Laser Ablation. Experiments were first done with normal D_2 because it forms a more robust solid (FP 18.6 K).[5,36] Different laser energies were employed to optimize the signal to noise in the deuterium matrix infrared spectrum where the amount of gas that can be deposited and condensed quickly enough to trap product species is limited to 2.5−3.0 mmol. The major product absorptions are assigned to $(D_2)AuD$ at 1556.5 cm^{-1} and $(D_2)AuD_3$ at 1198.6 cm^{-1} in the upper region[5,10] and to AuD_2 at 457.0 cm^{-1} and $(D_2)AuD$ at 434.8 cm^{-1} in the lower region. The lower region of the infrared spectrum is shown in Figure 1. Note that ultraviolet $\lambda > 240$ nm irradiation using a mercury arc lamp (Philips, 175 W) increased $(D_2)AuD$ and AuD_2 absorptions. Final annealing to 9 K increased the 457.0 cm^{-1} band, which was first assigned[5,10] to the b_1 D-Au-D bending mode of $(D_2)AuD_3$, but is reassigned here to the bending mode of AuD_2.

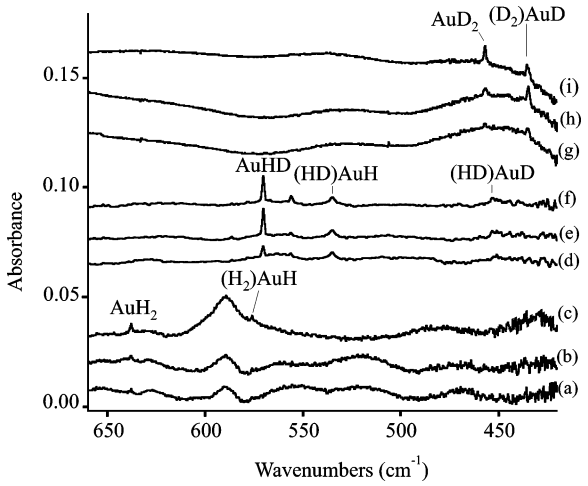

Figure 1. Infrared spectra in the 660−420 cm^{-1} region for laser-ablated Au co-deposited with pure hydrogen isotopic samples at 3.5 K for 25 min. (a) Au + H_2, (b) after $\lambda > 240$ nm photolysis, (c) after annealing to 6.4 K, (d) Au + HD, (e) after $\lambda > 240$ nm photolysis, (f) after annealing to 7.5 K, (g) Au + D_2, (h) after $\lambda > 240$ nm photolysis, and (i) after annealing to 9.0 K.

Investigations were subsequently done with normal H_2, which forms a softer, more volatile solid (FP 14.0 K)[36] at the 3.5 K substrate temperature. The amount of gas deposited is 2.0−2.5 mmol, and the fraction actually condensed is less than for D_2 in these experiments. The major product absorptions are assigned to $(H_2)AuH$ at 2164 cm^{-1} and $(H_2)AuH_3$ at 1661.5 cm^{-1} in the upper region and to AuH_2 at 638.1 cm^{-1} and $(H_2)AuH$ at 576.0 cm^{-1} in the lower region.[6,37] Again, ultraviolet photolysis and annealing had the same effect on the H as the D substituted products.

One experiment was done with HD (FP 16.6 K) for product identification, and the major product absorptions are (HD)AuH at 2162.7 cm^{-1} and (HD)AuD at 1555.2 cm^{-1} in the upper region and AuHD at 570.6 cm^{-1} in the lower region. Here, $\lambda > 470$, 380, and 290 nm light do not change the 570.6 cm^{-1} band, but $\lambda > 240$ nm irradiation doubles this absorption.

Thermal Evaporation. After several experiments, it became obvious from the brown-tan sample color that a higher gold deposition rate as measured by microbalance could be used for D_2 than for H_2 because of the greater condensation efficiency of D_2 compared to H_2. Typically, co-deposited samples showed no reaction products in the infrared spectra.[38] Because of the fortunate coincidence between the strong mercury emission line at 265 nm and the $^2P_{1/2}$ absorption of gold atoms measured in solid deuterium at 263 nm and solid hydrogen at 265 nm,[38,39] selective resonance excitation of Au could be done using a dielectric notch filter and the simple Au($^2P_{1/2}$) + H_2 (solid, 3.5 K) reaction products could be observed and characterized. New infrared bands include strong 2164.2 cm^{-1} $(H_2)AuH$ absorption in the upper region[37] and weaker 638.1 cm^{-1} AuH_2 and 575.6 cm^{-1} $(H_2)AuH$ absorptions in the lower region for hydrogen

TABLE 1: Structure and Vibrational Frequencies Calculated for the $^2B_2$ Ground State of AuH_2 Using Density Functional Theory and Relativistic Pseudopotentials for Gold

funct/pseudopot	Å, deg	frequencies, cm^{-1} (intensities, km/mol)
BPW91/LANL2DZ[a]	1.617, 129.1	AuH_2: 1941.7 (a_1, 1.3), 1636.8 (b_2, 0.3), 649.8 (a_1, 28) AuHD: 1819.7 (0.9), 1238.6 (0.3), 564.5 (22) AuD_2: 1374.9 (0.7), 1162.6 (0.2), 461.5 (14)
B3LYP/LANL2DZ[a]	1.618, 128.8	AuH_2: 1938.8 (a_1, 1.7), 1634.1 (b_2, 0.9), 649.2 (a_1, 36)
BPW91/SDD[a]	1.619, 129.1	AuH_2: 2003.8 (a_1, 1), 1758.0 (b_1, 0.5), 666.5 (a_1, 25) AuD_2: 1418.9 (0.5), 1248.7 (0.2), 473.4 (12)
B3LYP/SDD[a]	1.619, 128.6	AuH_2: 1995.2 (a_1, 2), 1742.1 (b_1, 1), 666.5 (a_1, 33)
BPW91/SDD[b]	1.616, 129.5	AuH_2: 2009.0 (a_1, 1.0), 1758.6 (b_2, 0.5), 677.5 (a_1, 24)
B3LYP/SDD[b]	1.617, 128.8	AuH_2: 2002.9 (a_1, 1.7), 1745.5 (b_1, 0.7), 676.1 (a_1, 33)

[a] 6-311++G(d, p) basis for H. [b] 6-311++G(3dp, 3df) basis for H.

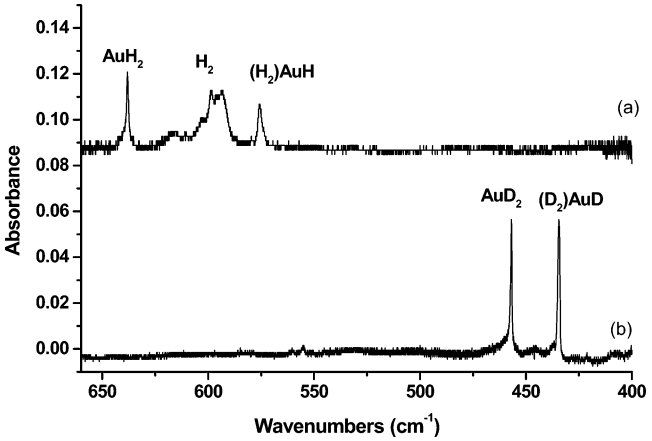

Figure 2. Infrared spectra in the 650−400 cm^{-1} region for thermally evaporated gold co-deposited with hydrogen on a copper surface near 3 K. Plotted spectra are difference spectrum after 265-nm dielectric spike filter resonance photolysis minus spectrum of deposited sample before photolysis. Spectra recorded at 0.1 cm^{-1} resolution on bolometer detector (a) Au + H_2 and (b) Au + D_2.

and the corresponding 1556.5, 457.0, and 434.5 cm^{-1} bands for the deuterated products.[5] Spectra from the lower region are shown in Figure 2.

DFT Calculations. DFT calculations performed for AuH_2 using the BPW91 and B3LYP functionals and SDD relativistic ECP for gold gave structures in agreement with the earlier MRSDCI computations.[4] Of particular relevance here, both functionals predicted a strong valence angle bending mode near 660 cm^{-1} in the infrared spectrum and very weak stretching modes in the 2000−1700 cm^{-1} region. Similar calculations were performed with the LANL2DZ relativistic ECP for gold, and the structures are virtually the same. The calculated bending frequencies were predicted 17 cm^{-1} lower and the stretching frequencies were 60−120 cm^{-1} lower using LANL2DZ. The larger 6-311++G(3df, 3dp) basis set for H gave 3−10 cm^{-1} higher frequencies. With all DFT calculations, the stretching modes are predicted to be 20× weaker than the bending mode (Table 1). The spectra were examined in the computed stretching regions: the symmetric stretching mode of AuH_2 cannot be stronger than 4% of the 638 cm^{-1} band and the a_1 stretching mode of AuD_2 cannot exceed 8% of the 457.0 cm^{-1} band on the basis of observed signal to noise. Hence, we can assign the 638, 570, and 457 cm^{-1} absorptions to the bending modes of AuH_2, AuHD, and AuD_2, respectively, with confidence.

MP2 and CCD Calculations. Table 2 lists the optimized geometries, vibrational frequencies, and IR intensities of the X^2B_2 ground state of AuH_2 using the MP2 and CCD methods with different basis sets. As seen from Table 2, the optimized geometries of different methods are close with the exception

TABLE 2: Optimized Structure and Vibrational Frequencies Calculated for the $^2B_2$ Ground State of AuH_2 at Various Levels

method	basis	Au−H	θ	(a_1)	(b_2)	(a_1)
CCD	Au(3s3p4d1f) H(CCPVTZ)	1.600	123.5	2071.9 (2.7)	1800.4 (0.09)	670.5 (60)
MP2	Au(3s3p4d1f) H(CCPVTZ)	1.591	123.9	2084.9	1814.2	651.1
MP2	Au(3s3p4d) H(CCPVTZ)	1.568	122.7	2177.5 (7.1)[a]	1868.6 (0.005)[a]	773.3 (62)[a]
CCD	Au(3s3p4d2f) H(CCPVTZ)	1.603	123.3	2047 (2.0)[a]	1770 (0.48)[a]	662 (61)[a]
MP2	Au(3s3p4d2f) H(CCPVTZ)	1.593	123.8	2056.2	1777.8	639

[a] The IR intensities of the modes in kJ/mol. The MP2 method with 4f gives unrealistic IR intensities.

that the including of the first 4f function elongates the Au−H bond by 0.02 Å at the MP2 level and by 0.002−0.003 Å for the second 4f function at MP2 and CCD level. The vibrational frequencies are a bit more sensitive to the level of theory, and we consider the CCD method with gold (3s3p4d2f) basis set: the b_2 frequency goes down as the level of theory goes up. The AuH_2 bending mode is the only observable frequency and accurate prediction requires the f function.

CASSCF/MRSDCI Calculations of the Bending Potential Energy Surfaces. Figure 3 shows our computed potential energy surfaces of three AuH_2 electronic states together with various dissociation limits. The X^2B_2 ground state adiabatically dissociates into Au(^{2}D) + H_2 and forms a bent obtuse minimum with a bond angle near 129°. The ^{2}S ground state of Au, on the other hand, has to surpass a huge barrier and forms only a linear $^2\Sigma_g^+$ state that is considerably higher energy than its dissociation products. Thus, the ground state of Au is unreactive toward H_2 as expected. In contrast to the silver atom, the first excited state of gold is ^{2}D while it is ^{2}P for Ag arising from the $4d^{10}5p^1$ configuration.[40] The corresponding state of Au is 4.9 eV higher than the ground state, while the ^{2}D state from $5d^96s^2$ configuration is only 1.7 eV above the ground state. This is a consequence of relativistic mass-velocity stabilization[31] of the 6s orbital of Au and the corresponding destabilization of the 5d orbital. Thus, relativistic effects are important for gold.[2−4,31,41,42]

The barrier to insert the Au(^{2}D) atom into H_2 is 53 kcal/mol as seen from Figure 3. However, the ^{2}P state of Au is considerably higher than this barrier. When the Au atom is excited to the ^{2}P state, it is very reactive because ^{2}P Au also yields a $^2B_2$ state, which undergoes avoided crossing with the $^2B_2$ state arising from the ^{2}D state of Au. The barrier in Figure 3 appears to arise from this avoided crossing. Moreover, the ^{2}P state of Au also results in other states such as $^2A_1$, which would cross the $^2B_2$ curve. At the crossing point, spin−orbit coupling will

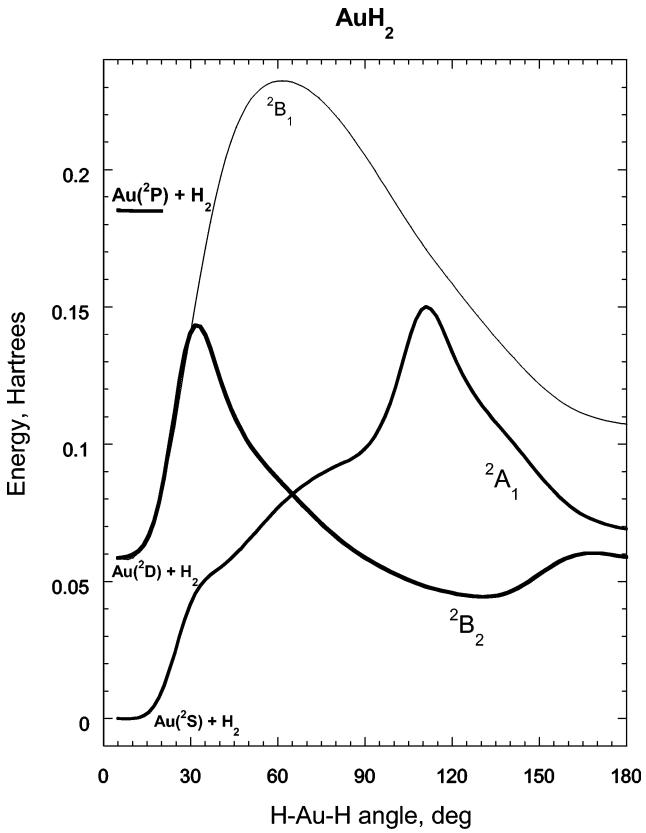

Figure 3. Bending potential surfaces for three electronic states of AuH_2 together with $Au(^2S) + H_2$, $Au(^2D) + H_2$, and $Au(^2P) + H_2$ dissociation limits.

provide a strong channel for the formation of the X^2B_2 state. The barrier for the formation of the lowest $^2A_1$ state from ^2S $Au + H_2$ is 95 kcal/mol.

As seen from Figure 3, once the X^2B_2 state is formed through excitation of the gold atom to the ^2P state, it will stay in the potential well as it has to surpass a large barrier to dissociate back to $Au(^2D) + H_2$. On the other hand, the crossing of the $^2B_2$ state with the $^2A_1$ state occurs at 65 deg. The crossing point is about 25 kcal/mol higher than the X^2B_2 minimum. Even if spin−orbit coupling between the two states is significant, the resulting barrier of 25 kcal/mol must be overcome before decomposition to $Au(^2S)$ and H_2. The spin−orbit coupling between the two states cannot be large since the $^2A_1$ state has predominantly $Au(5d^{10}6s^1)$ character, and thus the spin−orbit effect must be small for the $^2A_1$ state. Although the $^2B_2$ state will exhibit a larger spin−orbit effect, its coupling with $^2A_1$ should be negligible because of the closed $5d^{10}$ shell of Au in the $^2A_1$ state. We thus conclude that X^2B_2 is quite a long-lived ground state: it is 27 kcal/mol more stable than $Au(^2D) + H_2$.

While the computed bending potential energy surface of the $^2A_1$ state here is close to the previous study,[4] the $^2B_2$ surface differs especially near the dissociation and the minimum. This is primarily because the previous work[4] did not include excitations from the $5d^{10}$ electrons of Au, and thus the surface in the previous study dissociates into $Au(^2P) + H_2$. While this is true for Ag, the AuH_2 $^2B_2$ state dissociates differently when excitations from $5d^{10}$ are included at the CASSCF level.

Table 3 shows our computed MRSDCI geometries and energy separations of several electronic states of AuH_2. The MRSDCI geometries differ slightly from the MP2, CCSD, and DFT methods mainly because of the inclusion of multireferences in the MRSDCI while all other methods included only single

TABLE 3: The MRSDCI Properties of Electronic States of AuH_2

state	R_e (Å)	θ_e (deg)	E(eV)	expt (eV)[a]
$^2B_2$	1.635	128.8	0.77	
$^2\Sigma_u^+(^2B_2)$	1.728	180.0	1.60	
$^2\Sigma_g^+(^2A_1)$	1.675	180.0	1.82	
$^2B_1$	1.713	180.0	2.92	
$Au(^2S) + H_2$			0.0	0.0
$Au(^2D) + H_2$			1.95	1.74
$Au(^2P) + H_2$			5.03	4.91
$Au(^2S) + 2H$			4.6	4.75[b,c]

[a] All experimental atomic results are J-averaged atomic energy levels from ref 40. [b] Huber, K. P.; Herzberg, G. *Molecular Spectra and Molecular Structure, Vol. IV, Constants of Diatomic Molecules*; New York: Van Nostrand Reinhold, 1979. [c] Value includes zero-point correction of 6.4 kcal/mol.

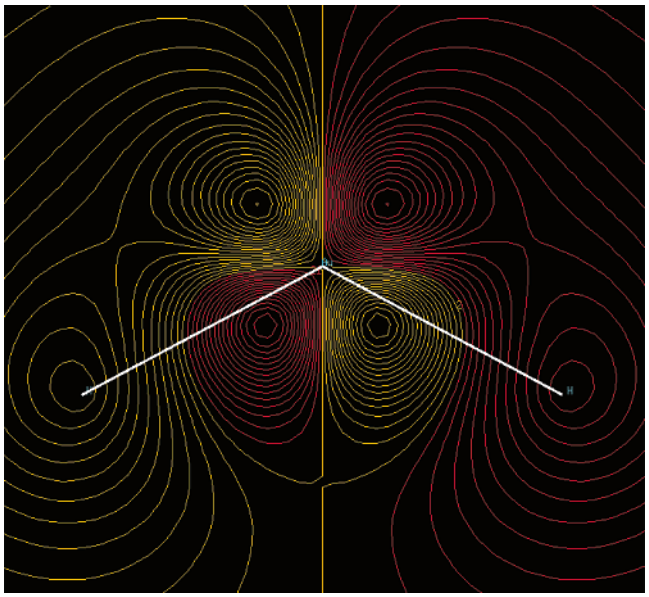

Figure 4. Two-dimensional electron density contour plot of the AuH_2 ground state. Calculation at MP2 level with 3s3p4d2f basis for gold and CCPVTZ basis for hydrogen.

references. Also, the barrier heights and dissociation energies are more correctly represented by CASSCF/MRSDCI than any other method. As seen from Table 3, our computed energy separations of the excited states of Au are in excellent agreement with experiment giving further confidence to the computed MRSDCI results.

Figures 4 and 5 illustrate computed electron density contour plots (MP2/3s3p4d2f/CCPVTZ) of the ground state of AuH_2 in two and three dimensions, respectively. The bent HAuH molecule is located by two lines joined at the Au atom. The plot reveals significant depletion of electronic charge density at the gold site. This is followed by donation of electronic charge from the Au(5d π) orbital back into the $1\sigma_u$ antibonding orbital of H_2. In fact, projecting the charge density on the plane of the molecule reveals considerable Au(5d π) interaction with the $1\sigma_u$ orbital. We thus conclude that the dissociation of H_2 in the excited state is assisted by the dative mechanism of electron transfer from the gold atom to the hydrogens and back transfer from the H_2 $1\sigma_u$ to Au (d π) and (p π). This is not feasible in the ground $Au(^2S)$ state, while it is possible in the $Au(^2D)$ excited state. This explains the smaller barrier for the formation of $^2B_2$ state of AuH_2 compared to the $^2A_1$ state.

Reaction Mechanisms. The important reaction observed here is the insertion of $Au(^2P)$ into dihydrogen. The excess energy

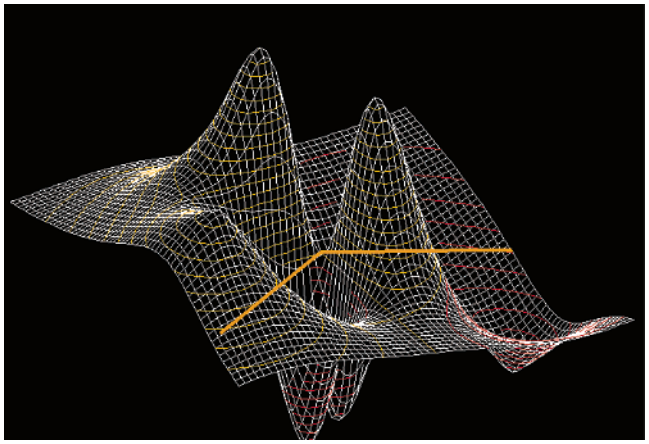

Figure 5. Electron density contour plot of the AuH_2 ground state. The plot is consistent with a dative electron-transfer mechanism of dissociation, where Au transfers electronic charge to the hydrogen atoms and there is back transfer from the H_2 $1\sigma_u$ orbital to the Au(5d π) orbital. Calculation at MP2 level with 3s3p4d2f basis for gold and CCPVTZ basis for hydrogen. The HAuH molecule is located by lines intersecting at the Au center.

is provided by mercury arc emission at 265 nm or by laser ablation.[43] Reaction initiation by resonance absorption using a narrow band filter verifies this mechanism. Once formed, the AuH_2 molecule is stable owing to the barrier to dissociation into lower energy and unreactive Au(^{2}S) and H_2.

$$Au(^2S) + H_2 \xrightarrow{265\ nm} Au(^2P) + H_2 \rightarrow AuH_2(^2B_2) \quad (1)$$

Finally, AuH_2 has a significant electron affinity (estimated as 68 kcal/mol by DFT), and the AuH_2^- anion has been observed in laser-ablation experiments.[6]

Conclusions

The novel AuH_2 molecule has been formed in solid hydrogen by reactions of excited gold atoms from laser ablation and thermal evaporation. The AuH_2 molecule is separated by a 53 kcal/mol barrier from Au(^{2}D) + H_2 decomposition products. The bending modes of AuH_2, AuHD, and AuD_2 have been observed at 638.1, 570.6, and 457.0 cm^{-1}. These frequencies and the lack of infrared intensity in the stretching modes are in agreement with the results of relativistic ECP, DFT, MP2, and CCD calculations. We find that the X^2B_2 state of AuH_2 has a stability of 27 kcal/mol relative to Au(^{2}D) + H_2 and is expected to be long-lived in this state because of a large barrier to dissociation. Unlike the X^2B_2 state of AgH_2 which dissociates into Ag(^{2}P) + H_2, the corresponding state of AuH_2 dissociates into Au(^{2}D) + H_2. This is a consequence of the fact that the first excited state of Au atom is ^{2}D, while it is ^{2}P for silver, which is attributed to relativistic stabilization[31] of the 6s orbital of Au and destabilization of the 5d orbital.

Acknowledgment. We gratefully acknowledge support for this work from N.S.F grant CHE 00-78836, and the assistance of D. Carrére and D. Danset with thermal gold experiments performed in Paris. The work at UC Davis was supported by the office of basic energy sciences, chemical sciences division of U.S. Department of Energy under grant no. DEFG02-86ER13558, and the work at LLNL was carried out under the auspices of U.S. Department of Energy under contract no. W-7405-Eng-48.

References and Notes

(1) Cotton, F. A.; Wilkinson, G.; Murillo, C. A.; Bochmann, M. *Advanced Inorganic Chemistry*, 6th ed.; Wiley: New York, 1999.
(2) Pyykkö, P. *Chem. Rev.* **1988**, *88*, 563.
(3) Schwerdtfeger, P.; Schwarz, W. H. E.; Bowmaker, G. A.; Boyd, P. D. W. *J. Chem. Phys.* **1989**, *91*, 1762 and references therein.
(4) Balasubramanian, K.; Liao, M. Z. *J. Phys. Chem.* **1988**, *92*, 361.
(5) Wang, X.; Andrews, L. *J. Phys. Chem. A* **2002**, *106*, 3744 (Au + H_2).
(6) Andrews, L.; Wang, X. *J. Am. Chem. Soc.* **2003**, *125*, 11751.
(7) Schwerdtfeger, P.; Boyd, P. D. W.; Brienne, S.; Burrell, A. K. *Inorg. Chem.* **1992**, *31*, 3411 and references therein.
(8) (a) Bayse, C. A.; Hall, M. B. *J. Am. Chem. Soc.* **1999**, *121*, 1348. (b) Bayse, C. A. *J. Phys. Chem. A* **2001**, *105*, 5902.
(9) Balabanov, N. B.; Boggs, J. E. *J. Phys. Chem. A* **2001**, *105*, 5906.
(10) Wang, X.; Andrews, L. *J. Am. Chem. Soc.* **2001**, *123*, 12899.
(11) Griffiths, M. J.; Barrow, R. F. *J. Chem. Soc., Faraday Trans.* **1977**, *73*, 943.
(12) Citra, A.; Andrews, L. *J. Mol. Struct. (THEOCHEM)* **1999**, *49*, 95.
(13) Schröder, D.; Brown, R.; Schwerdtfeger, P.; Wang, X. B.; Yang, X.; Wang, L. S.; Schwarz, H. *Angew. Chem., Int. Ed.* **2003**, *42*, 311.
(14) Yamaguchi, Y.; Schaefer, H. F., III. *Chem. Phys.* **1997**, *225*, 23 and references therein.
(15) Yamaguchi, Y.; Schaefer, H. F., III. *J. Chem. Phys.* **1997**, *106*, 8753 and references therein.
(16) Andrews, L. *J. Chem. Phys.* **1969**, *50*, 4288.
(17) Allen, W. D.; Horner, D. A.; DeKock, R. L.; Remington, R. B.; Schaefer, H. F., III. *Chem. Phys.* **1989**, *133*, 11, and references therein.
(18) Liang, C.; Davy, R. D.; Schaeffer, H. F., III. *Chem. Phys. Lett.* **1989**, *159*, 393.
(19) Wang, X.; Andrews, L.; Tam, S.; DeRose, M. E.; Fajardo, M. E. *J. Am. Chem. Soc.* **2003**, *125*, 9218.
(20) Liang, B.; Andrews, L. *J. Phys. Chem. A* **2000**, *104*, 9156.
(21) Andrews, L.; Citra, A. *Chem. Rev.* **2002**, *102*, 885.
(22) Andrews, L.; Wang, X.; Alikhani, M. E.; Manceron, L. *J. Phys. Chem. A* **2001**, *105*, 3052 (Pd + H_2).
(23) Tremblay, B.; Manceron, L. *Chem. Phys.* **1999**, *250*, 187.
(24) Goubet, M.; Asselin, P.; Manceron, L.; Soulard, P.; Perchard, J.-P. *Phys. Chem. Chem. Phys.* **2003**, *5*, 3591.
(25) Frisch, M. J.; Trucks, G. W.; Schlegel, H. B.; Scuseria, G. E.; Robb, M. A.; Cheeseman, J. R.; Zakrzewski, V. G.; Montgomery, J. A., Jr.; Stratmann, R. E.; Burant, J. C.; Dapprich, S.; Millam, J. M.; Daniels, A. D.; Kudin, K. N.; Strain, M. C.; Farkas, O.; Tomasi, J.; Barone, V.; Cossi, M.; Cammi, R.; Mennucci, B.; Pomelli, C.; Adamo, C.; Clifford, S.; Ochterski, J.; Petersson, G. A.; Ayala, P. Y.; Cui, Q.; Morokuma, K.; Malick, D. K.; Rabuck, A. D.; Raghavachari, K.; Foresman, J. B.; Cioslowski, J.; Ortiz, J. V.; Stefanov, B. B.; Liu, G.; Liashenko, A.; Piskorz, P.; Komaromi, I.; Gomperts, R.; Martin, R. L.; Fox, D. J.; Keith, T.; Al-Laham, M. A.; Peng, C. Y.; Nanayakkara, A.; Gonzalez, C.; Challacombe, M.; Gill, P. M. W.; Johnson, B.; Chen, W.; Wong, M. W.; Andres, J. L.; Gonzalez, C.; Head-Gordon, M.; Replogle, E. S.; Pople, J. A. *Gaussian 98*, revision A.6; Gaussian, Inc.: Pittsburgh, PA, 1998.
(26) (a) Becke, A. D. *Phys. Rev. A* **1988**, *38*, 3098. (b) Perdew, J. P.; Wang, Y. *Phys. Rev. B* **1992**, *45*, 13244.
(27) (a) Becke, A. D. *J. Chem. Phys.* **1993**, *98*, 5648. (b) Lee, C.; Yang, W.; Parr, R. G. *Phys. Rev. B* **1988**, *37*, 785.
(28) (a) Krishnan, R.; Binkley, J. S.; Seeger, R.; Pople, J. A. *J. Chem. Phys.* **1980**, *72*, 650. (b) Frisch, M. J.; Pople, J. A.; Binkley, J. S. *J. Chem. Phys.* **1984**, *80*, 3265.
(29) Wadt, W. R.; Hay, P. J. *J. Chem. Phys.* **1985**, *82*, 284.
(30) Legge, F. S.; Nyberg, G. L.; Peel, J. B. *J. Phys. Chem. A* **2001**, *105*, 7905.
(31) Balasubramanian, K. *Relativistic Effects in Chemistry: Part A Theory and Techniques*; Wiley-Interscience: New York, 1997; p 301.
(32) Balasubramanian, K. *Relativistic Effects in Chemistry: Part B Applications*; Wiley-Interscience: New York, 1997; p 527.
(33) Balasubramanian, K. *Chem. Phys. Lett.* **1986**, *127*, 324.
(34) The major authors of *ALCHEMY II* are B. Liu and M. Yoshimine.
(35) Balasubramanian, K. *J. Chem. Phys.* **2000**, *112*, 7425.
(36) Silveri, I. F. *Rev. Mod. Phys.* **1980**, *52*, 393.
(37) Wang, X.; Andrews, L.; Manceron, L.; Marsden, C. *J. Phys. Chem. A* **2003**, *107*, 8492.
(38) Gruen, D. M.; Bates, J. K. *Inorg. Chem.* **1977**, *16*, 2450.
(39) Abe, H.; Schulze, W.; Kolb, D. M. *Chem. Phys. Lett.* **1979**, *60*, 208.
(40) Moore, C. E. *Atomic Energy Levels*, *Vol III*; National Bureau of Standards: Washington, DC, 1971.
(41) Pyykkö, P. *Nature* **1977**, *266*, 337.
(42) Pyykkö, P. *Angew. Chem., Int. Ed.* **2004**, in press.
(43) Kang, H.; Beauchamp, J. L. *J. Phys. Chem.* **1985**, *89*, 3364.